NASA TECHNICAL NOTE

NASA TN D-8136

NASA TN D-8136

SUBSONIC STABILITY AND CONTROL DERIVATIVES FOR AN UNPOWERED, REMOTELY PILOTED 3/8-SCALE F-15 AIRPLANE MODEL OBTAINED FROM FLIGHT TEST

Kenneth W. Iliff, Richard E. Maine, and Mary F. Shafer

Flight Research Center
Edwards, Calif. 93523

NATIONAL AERONAUTICS AND SPACE ADMINISTRATION • WASHINGTON, D. C. • JANUARY 1976

1. Report No. NASA TN D-8136	2. Government Accession No.	3. Recipient's Catalog No.
4. Title and Subtitle SUBSONIC STABILITY AND CONTROL DERIVATIVES FOR AN UNPOWERED, REMOTELY PILOTED 3/8-SCALE F-15 AIRPLANE MODEL OBTAINED FROM FLIGHT TEST		5. Report Date January 1976 6. Performing Organization Code
7. Author(s) Kenneth W. Iliff, Richard E. Maine, and Mary F. Shafer		8. Performing Organization Report No. H-905
9. Performing Organization Name and Address NASA Flight Research Center P.O. Box 273 Edwards, California 93523		10. Work Unit No. 512-53-03 11. Contract or Grant No.
12. Sponsoring Agency Name and Address National Aeronautics and Space Administration Washington, D.C. 20546		13. Type of Report and Period Covered Technical Note 14. Sponsoring Agency Code
15. Supplementary Notes		

16. Abstract

In response to the interest in airplane configuration characteristics at high angles of attack, an unpowered remotely piloted 3/8-scale F-15 airplane model was flight tested. This report documents the subsonic stability and control characteristics of this airplane model over an angle of attack range of -20° to 53°. The remotely piloted technique for obtaining flight test data was found to provide adequate stability and control derivatives. The remotely piloted technique provided an opportunity to test the aircraft mathematical model in an angle of attack regime not previously examined in flight test. The variation of most of the derivative estimates with angle of attack was found to be consistent, particularly when the data were supplemented by uncertainty levels.

17. Key Words (Suggested by Author(s))	18. Distribution Statement
F-15 airplane model Stability and control derivatives Remotely piloted research vehicle	Unclassified - Unlimited Category: 08

19. Security Classif. (of this report)	20. Security Classif. (of this page)	21. No. of Pages	22. Price*
Unclassified	Unclassified	31	$3.75

*For sale by the National Technical Information Service, Springfield, Virginia 22161

SUBSONIC STABILITY AND CONTROL DERIVATIVES FOR AN UNPOWERED, REMOTELY PILOTED 3/8-SCALE F-15 AIRPLANE MODEL OBTAINED FROM FLIGHT TEST

Kenneth W. Iliff, Richard E. Maine, and Mary F. Shafer
Flight Research Center

INTRODUCTION

The increased concern with airplane characteristics at high angles of attack during stall, departure, and spin has motivated research in this angle of attack regime. There is a lack of complete confidence in the ability of current design methods to predict airplane handling qualities at high angles of attack, so experimental as well as analytical data are needed. The prediction of the handling qualities of an airplane relies to a large extent on the prediction of its stability and control characteristics. The proof of a new design must await flight tests, when the measured airplane stability and control characteristics can be compared with those estimated before flight test. The design cycle is reasonably well understood for low speeds and angles of attack for normal maneuvering, but the desire to utilize high angles of attack has expanded design envelopes beyond previously accepted design limits.

In response to the interest in stall, departure, and spin controllability, the NASA Flight Research Center is flight testing an unpowered remotely piloted 3/8-scale model of the F-15 airplane to high angles of attack. The remotely piloted flight test technique (ref. 1) was chosen because of the risks involved in aircraft spin testing. The technique is versatile in that the pilot interacts with the vehicle as he does during normal flight, it is potentially more economical than full-scale flight testing, and it allows the flight envelope to be expanded more rapidly than do conventional flight test methods. The derivative characteristics determined during the flight program were used both to verify the predicted airplane model aerodynamics and to update a flight support simulator.

This report documents the stability and control derivatives of the F-15 airplane model determined at subsonic speeds over an angle of attack range from -20° to 53°.

SYMBOLS

a_n	normal acceleration, g
a_Y	lateral acceleration, g
C_l	rolling-moment coefficient
C_m	pitching-moment coefficient
C_{m_0}	pitching-moment coefficient for zero α and zero δ_e
C_N	normal-force coefficient
$C_{N_{trim}}$	normal-force coefficient at trim for the center of gravity at 26-percent mean aerodynamic chord
C_{N_0}	normal-force coefficient for zero α and zero δ_e
C_n	yawing-moment coefficient
C_Y	side-force coefficient
I_X	moment of inertia about the longitudinal axis, $kg\text{-}m^2$
I_{XZ}	cross product of inertia, $kg\text{-}m^2$
I_Y	moment of inertia about the lateral axis, $kg\text{-}m^2$
I_Z	moment of inertia about the normal axis, $kg\text{-}m^2$
p	roll rate, deg/sec or rad/sec
q	pitch rate, deg/sec or rad/sec
r	yaw rate, deg/sec or rad/sec
t	time, sec
W	weight, N
α	angle of attack of the body axis, deg

α_0	angle of attack of the principal axis, deg
β	angle of sideslip, deg
$\dot{\beta}$	time derivative of angle of sideslip, rad/sec
δ_a	aileron deflection, deg
δ_d	differential tail deflection, deg
δ_e	elevator deflection, deg
$\delta_{e_{trim}}$	elevator deflection at trim for the center of gravity at 26-percent mean aerodynamic chord
δ_r	rudder deflection, deg
θ	pitch angle, deg
φ	roll angle, deg

Subscripts:

$p, q, r, \alpha, \beta, \dot{\beta}, \delta_a, \delta_d, \delta_e, \delta_r$	partial derivative with respect to the subscripted variable

DESCRIPTION OF THE VEHICLE AND INSTRUMENTATION

The F-15 airplane is a conventional single-placed two-engined fighter with the wing leading edge swept back 45° and twin vertical tails. The model (figs. 1 and 2) and the full-scale F-15 aircraft have similar elevator, aileron, and rudder control surfaces for the stability augmentation system and for pilot control. The elevator is used for longitudinal control, and the rudder, wing aileron, and differential elevator are used for lateral-directional control. The model is unpowered, and the inlets are blocked. Pertinent airplane model physical characteristics are presented in table 1. Details concerning the airplane model are given in reference 1. The implementation of the remote piloting and stability augmentation aspects of the vehicle are given in reference 2.

Two model configurations were tested: the basic configuration and the so-called production configuration. The production configuration updated the basic configuration to that of the full-scale production airplane. This configuration was used during the last seven flights. The differences between the two versions of the model are shown in figure 3. The changes (shown dashed) involved rounding the wingtip trailing edges and removing the section of the horizontal stabilizer shown in the figure. The airplane model was flown with three center of gravity locations —

TABLE 1. - THREE-EIGHTHS-SCALE MODEL CHARACTERISTICS

Model -	
Length, m	7.15
Weight, N	10,964
Wing -	
Area, m^2	7.94
Span, m	4.89
Aspect ratio	3.0
Mean aerodynamic chord, m	1.82
Leading-edge sweep, deg	45.0
Taper ratio	0.25
Dihedral, deg	-1.0
Incidence, deg	0
Ailerons:	
Span, m	1.24
Deflection, deg	±20
Horizontal tail -	
Planform (exposed), m^2	1.57
Span, m	3.24
Aspect ratio	2.05
Taper ratio	0.34
Leading-edge sweep, deg	50.0
Mean aerodynamic chord (exposed), m	0.94
Dihedral, deg	0
Tail length, m	2.30
Deflection, deg:	
Symmetrical	15, -26
Differential	±11
Vertical tails -	
Area (both sides), m^2	1.64
Span, m	1.18
Leading-edge sweep, deg	36.6
Mean aerodynamic chord, m	0.77
Tail length, m	2.02
Rudders -	
Area (total), m^2	0.26
Span, m	0.54
Mean aerodynamic chord, m	0.24
Maximum deflection, deg	±30

26-percent, 30.3-percent, and 38.5-percent mean aerodynamic chord. The location of the center of gravity is indicated by the configuration's designation, as shown in table 2. Table 2 also shows the configuration inertias.

The airplane model's instrumentation consisted of the standard package used for the measurement of stability and control parameters, including three-axis angular rate gyros, attitude gyros, and linear accelerometers, along with control position sensors and boom-mounted angle of attack and angle of sideslip vanes. The data were filtered with 40-hertz passive analog filters. The data were then sampled with a 9-bit pulse code modulation system and telemetered to a ground station in real time to be recorded. Before the flight data were analyzed, corrections for upwash and sidewash were made to the angle of attack and angle of sideslip measurements. The corrections to angle of attack and angle of sideslip for angular rates, as well as those for accelerometer position, were included in the digital program used for the derivative extraction. A complete description of the instrumentation system, including the accuracy and resolution of each quantity measured, is given in reference 1.

TABLE 2. - INERTIA AND WEIGHT CHARACTERISTICS

Configuration	Center of gravity, percent mean aerodynamic chord	I_X, kg-m^2	I_Y, kg-m^2	I_Z, kg-m^2	I_{XZ}, kg-m^2	W, N
Basic 1	26	373	2,579	3,021	16	10,960
Basic 2	30.3	373	2,451	2,893	3	10,960
Production 1	30.3	369	2,451	2,889	3	10,950
Production 2	38.5	369	2,402	2,839	0	9,119

FLIGHT TEST PROCEDURE

The 3/8-scale F-15 airplane model was air launched from a modified B-52 airplane at an altitude of approximately 15,000 meters at a Mach number of 0.65. After the launch, the pilot flew the aircraft remotely through a planned flight profile. In addition to maneuvers like stalls and spins, the pilot performed maneuvers for obtaining stability and control derivatives. These maneuvers were performed either by pilot commands through conventional cockpit controls or through an input pulse panel. The input pulse panel switch initiated programed control inputs once a desired flight condition was attained. These programed inputs allowed more maneuvers to be performed and permitted the pilot to concentrate on keeping flight conditions more nearly constant.

MANEUVERS AND FLIGHT CONDITIONS

The results presented in this report were obtained from 168 maneuvers that were performed during 12 of the first 16 flights of the airplane model. The remotely piloted research vehicle technique made maneuvers from which stability and control derivatives could be extracted possible over an angle of attack range of -20° to 53°, a range never before investigated in flight tests. The maneuvers were made at Mach numbers below 0.60. The maneuvers were performed for small perturbation analysis about the desired steady state flight condition, where linearity of the airplane model could be assumed. The maneuvers were initiated with inputs in the longitudinal or lateral-directional mode and analyzed for that mode. Most of the data were obtained without the stability augmentation system engaged in the mode to be analyzed; however, the stability augmentation system was engaged in the other mode when the vehicle was difficult to stabilize. Stabilized flight conditions were difficult to maintain at extreme angles of attack.

A consequence of the model's lack of power was that the high angle of attack maneuvers were of short duration. The shortness of the maneuvers sometimes reduced the accuracy of the estimates of the stability and control derivatives, which were defined by the mathematical model described in reference 3. Coupling motions, present in some high angle of attack maneuvers, were accounted for as described in

reference 4 to make it possible to determine stability and control derivatives adequately.

Most of the maneuvers that did not result in satisfactory matches were made at high angles of attack. There was some aerodynamic flow separation above an angle of attack of 15°, and the separation was quite extensive above an angle of attack of 25°. The results presented for angles of attack greater than 30° are the best available but may be affected by nonlinearities.

METHOD OF ANALYSIS

A maximum likelihood estimation method of analysis was used to determine the stability and control derivatives from the maneuvers made in flight. The method used (sometimes called the Newton-Raphson method) is an iterative technique that minimizes the difference between the aircraft's measured and computed response by adjusting the stability and control derivative values used in calculating the computed response. The Newton-Raphson method is used to attain the minimizations. The maximum likelihood estimation method can be modified to include *a priori* information from previous calculations, flight tests, or wind tunnel tests. The modification is made by including a penalty for adjusting the unknown stability and control derivatives away from the *a priori* values. Therefore, if new information is contained in a flight maneuver, the estimate of the derivative is affected only slightly by the *a priori* information. If no new information is contained in a flight maneuver, the *a priori* value results. This method is called modified maximum likelihood estimation and is fully described in reference 3. In this flight test program, *a priori* information was included in the analysis. A complete description and FORTRAN listings of the digital program used for the derivative extraction are given in reference 5.

In addition to providing estimates of the derivatives, this method of analysis provides uncertainty levels associated with each derivative. Uncertainty levels are proportional to the approximation of the Cramèr-Rao bounds described in reference 3 and are analogous to standard deviations of the estimated derivatives. The larger the uncertainty level, the greater the uncertainty in the estimated derivative. The most valid estimate of a derivative can be determined by comparing the uncertainty levels for the same derivative obtained from different maneuvers. The uncertainty levels in this way provide additional information about the validity of a derivative estimate.

RESULTS AND DISCUSSION

Data from 136 of the 168 maneuvers resulted in acceptable matches between the computed and measured time histories. Of the maneuvers that produced acceptable matches, 61 were longitudinal and 75 were lateral directional.

Computed and flight time histories for typical longitudinal and lateral-directional maneuvers are compared in figures 4(a) and 4(b). The results of the estimation of the stability and control derivatives are given for the longitudinal mode in figure 5

and for the lateral-directional mode in figure 6. Each symbol in figures 5 and 6 indicates an estimate made from one maneuver. The vertical line associated with each symbol indicates the uncertainty level associated with the estimate. The more valid estimates are readily identifiable by short vertical lines. A more complete explanation of the interpretation of uncertainty levels is given in reference 4.

The flight center of gravity position was constant for each flight. For the production configuration, all the data shown for angles of attack less than 38° were acquired with the center of gravity at 30.3-percent mean aerodynamic chord. For angles of attack greater than 38°, the data were acquired with the center of gravity at 38.5-percent mean aerodynamic chord. All the data were corrected to 26-percent mean aerodynamic chord.

Some of the scatter in the derivatives may be due to differences in trim stabilizer position, which were not corrected for. The trim deflection of the horizontal stabilizer for a given angle of attack was different for each center of gravity position. The stabilizer position above an angle of attack of 30° was -23° plus or minus 4.5°.

Flight conditions at high angles of attack often varied significantly. This made matching the maneuvers more difficult and could have contributed to the apparent nonlinearities. Because of the uncertainties in the data for high angles of attack ($\alpha > 30°$), the fairings for these data are dashed in the figures. If discrepancies existed in data near the same flight condition, fairings were determined by referring to the quality of the match in addition to the uncertainty levels.

Longitudinal Derivatives

The subsonic longitudinal stability and control derivatives, elevator position for trimmed flight, $\delta_{e_{trim}}$, and trimmed total normal-force coefficient, $C_{N_{trim}}$, are presented as a function of angle of attack in figure 5. Figure 5(a) summarizes the slope of the normal-force coefficient with angle of attack, C_{N_α}, and the static stability derivative, C_{m_α}, for the angle of attack range tested. Note that C_{N_α} is well defined, in that a fairing passes within all of the uncertainty level bounds. The maximum value of the derivative occurs at an angle of attack of approximately 8°. The values decrease somewhat as angle of attack increases and the wing flow separation becomes more extensive. The estimates of the static stability derivative, C_{m_α}, at all angles of attack are remarkably consistent. The configuration was stable at large negative angles of attack and became almost neutrally stable near an angle of attack of -10°. Static stability then increased up to an angle of attack of approximately 25°. The level of static stability appeared to be nearly constant at the highest angles of attack.

The longitudinal control effectiveness derivative, $C_{m_{\delta_e}}$, and the damping derivative, C_{m_q}, are shown in figure 5(b). Longitudinal control effectiveness was

nearly constant at -0.01 per degree for all angles of attack.

The longitudinal damping derivative showed somewhat greater variability with angle of attack, from small positive values at the most negative angles of attack for which data were obtained to a value of approximately -7 per radian in the normal operating angle of attack range. The damping derivative appears to approach zero at an angle of attack of approximately 25°, but positive damping (negative C_{m_q}) was indicated at greater angles of attack.

The normal-force coefficient due to longitudinal control deflection, $C_{N_{\delta_e}}$ (fig. 5(c)), shows much more uncertainty throughout the tested angle of attack range. This is not surprising, because the derivative is normally small for airplanes with separate wing and tail surfaces and is therefore difficult to determine. The locations of the data points and uncertainty levels do permit a fairing to be made with confidence, however.

The trim elevator position, $\delta_{e_{trim}}$, and trimmed total normal-force coefficient, $C_{N_{trim}}$, were computed from the stability and control derivatives and C_{N_0} and C_{m_0} for each maneuver and are presented in figure 5(d). Since $\delta_{e_{trim}}$ and $C_{N_{trim}}$ were computed, no uncertainty levels are shown. The data correctly show that the design maximum elevator deflection of -27.5° allowed a trim angle of attack of approximately 32° with the center of gravity at 26-percent mean aerodynamic chord. At angles of attack above 32°, more $\delta_{e_{trim}}$ was necessary to trim the airplane model than was available, so data for these angles of attack were obtained with the more rearward center of gravity positions (30.3-percent mean aerodynamic chord and 38.5-percent mean aerodynamic chord).

Lateral-Directional Derivatives

The lateral-directional stability and control derivatives are summarized in figure 6. There are many more estimates of the stability and damping derivatives than there are estimates of individual control derivatives, because stability and damping derivatives can be estimated from any maneuver, whereas a given control derivative can be estimated only from maneuvers where that control varies enough to have a significant effect. The large uncertainty levels are due to the large number of unknown lateral-directional derivatives and the difficulty of significantly exciting all the dynamic modes. The data are presented in figure 6 for the three center of gravity positions already mentioned (although effects of center of gravity position are not apparent) and for the two airplane model configurations. Consistent trends with angle of attack are apparent for all major derivatives, and in most cases fairings that pass through most of the uncertainty levels are possible. An exception among the major derivaties is C_{n_β}. This exception is discussed in Evidence of Nonlinearity.

Lateral-directional stability derivatives. - The directional stability derivative, C_{n_β} (fig. 6(a)), shows a good level of stability at low positive angles of attack but decreases to zero at an angle of attack of approximately 20°. Recovery to a positive value is indicated at the highest test angle of attack.

The dihedral effect derivative, C_{l_β} (fig. 6(a)), has a positive value at the most negative angles of attack and is generally negative for angles of attack greater than zero, with a maximum magnitude at an angle of attack of approximately 28°. The sign of C_{l_β} in figure 6(a) is desirable from a handling qualities standpoint for both positive and negative angles of attack.

The side-force derivative, C_{Y_β} (fig. 6(b)), is approximately -0.013 per degree for angles of attack up to approximately 20° and approximately -0.006 per degree at the higher angles of attack. This derivative is important for basic Dutch roll damping, and it contributes more for this airplane model than the rotary yaw damping derivative.

Control derivatives. - The variation of the control derivatives with angle of attack is presented in figures 6(c) to 6(g). The fairings are generally acceptable for all the control derivatives, with the possible exception of that for $C_{l_{\delta_r}}$ (fig. 6(c)), which exhibits some uncertainty in magnitude and sign in the angle of attack range from 20° to 40°. The derivative was definitely indicated to be small. Consistent data were obtained at the highest angles of attack for this derivative.

The estimates of the rudder effectiveness derivative, $C_{n_{\delta_r}}$ (fig. 6(c)), were generally consistent, but the values for the basic and production airplane model configurations were different in the angle of attack range from 0° to 40°. The maximum loss of rudder effectiveness was approximately 30 percent.

The yaw due to the roll control surface deflection derivatives ($C_{n_{\delta_d}}$ in fig. 6(d) and $C_{n_{\delta_a}}$ in fig. 6(e)) were positive up to an angle of attack of approximately 30°, where the aileron produced adverse yaw but the differential elevator control produced proverse yaw. The magnitude of the yaw due to the differential elevator control was approximately three times that produced by the ailerons.

The roll control effectiveness of the differential elevator deflection, $C_{l_{\delta_d}}$ (fig. 6(d)), was generally higher than the roll control effectiveness of the aileron, $C_{l_{\delta_a}}$ (fig.6(e)), at very low and high angles of attack. The magnitudes of the

derivatives were approximately equal in the angle of attack range from 5° to 10°. Some of the scatter in $C_{n_{\delta_d}}$ and $C_{l_{\delta_d}}$ for angles of attack from 15° to 30° may be due to differences in horizontal stabilizer postion.

The trends for $C_{Y_{\delta_r}}$, $C_{Y_{\delta_d}}$, and $C_{Y_{\delta_a}}$ (figs. 6(f) and 6(g)) are consistent, although the values are fairly small.

Rotary derivatives. - The roll and yaw damping derivatives are summarized in figures 6(h) and 6(i). Except for the damping-in-roll derivative, C_{l_p}, these derivatives have greater uncertainty levels than the stability and control derivatives. However, generally satisfactory fairings are possible through most of the uncertainty levels. The estimates and uncertainty levels of the yaw rate derivatives for angles of attack from 20° to 30° suggest that the effects of wing-separated flow on the vertical tails was great. The values of the derivatives are small in this angle of attack region. The results are somewhat more consistent at the highest angles of attack.

Reference 6 points out that at high angles of attack large values of $C_{n_{\dot{\beta}}}$ and $C_{l_{\dot{\beta}}}$ make significant contributions to the calculated aircraft response. To compensate for some of the scatter in C_{n_r} and C_{l_r}, the effect of including $C_{n_{\dot{\beta}}}$ and $C_{l_{\dot{\beta}}}$ as unknowns in the model was studied. It was found that $C_{n_{\dot{\beta}}}$ was linearly dependent on C_{n_r} and that $C_{l_{\dot{\beta}}}$ was linearly dependent on C_{l_r} for the data analyzed. Although reference 6 states the values of $C_{n_{\dot{\beta}}}$ and $C_{l_{\dot{\beta}}}$ to be relatively large in the wind tunnel, their effects on flight data were found to be insignificant in this investigation.

Sin α_0. - The lateral-directional equations of motion include a term $\sin \alpha_0 p$. This term can also be estimated as an unknown stability and control derivative. The parameter α_0 is the angle of attack of the principal axis. As can be seen from I_X, I_Z, and I_{XZ} in table 2, the body and principal axes are nearly coincident. Therefore, α_0 and α are essentially the same. The line plotted in figure 6(j) for $\sin \alpha_0$ versus α is $\sin \alpha$ versus α or perfect agreement between the estimate of $\sin \alpha$ and the measured angle of attack. It is apparent that the agreement is good, indicating that the measured angle of attack is probably also good.

Effects of Configuration

When stability and control data for the basic and production configurations were compared, it became apparent that the only derivatives significantly affected by the

difference in the configurations was $C_{n_{\delta_r}}$, where the production configuration showed somewhat reduced effectiveness.

Evidence of Nonlinearity

There is a considerable amount of scatter in some of the derivatives, although all the derivatives presented herein were obtained from good fits between the measured and computed data. The data are based on the assumption that the airplane mathematical model is linear. The scatter in the derivatives may be due to aircraft nonlinearities.

Nonlinearities may be observed in the estimates of control effectiveness: the airplane model usually responded proportionally more to small inputs than to large ones. This effect is particularly evident in $C_{m_{\delta_e}}$ (fig. 5(b)) for moderately high angles of attack (between 15° and 30°). The more negative values of $C_{m_{\delta_e}}$ were obtained from maneuvers with the smaller elevator deflections.

Another type of nonlinearity is apparent in the C_{n_β} derivative in figure 6(a) at an angle of attack of approximately 38°. The data show two levels for C_{n_β}, and the uncertainty levels are also larger in general at this angle of attack than at any other. The shaded symbols identify derivatives obtained from maneuvers performed a few seconds before an unexplained rapid rolloff or upset. Four of these upsets were observed during the flight program. One occurred at approximately the same angle of attack as the three shown, but no stability and control maneuvers were made immediately before the upset. The same upset phenomenon may have generated the data point that is unshaded but near the three shaded points. If so, some other occurrence prevented the upset. The greater negative values of C_{n_β} observed before the three upsets may explain what initiated the upsets: if the vortex flow generated by the forebody of the vehicle were no longer symmetric with respect to the airplane model's plane of symmetry, the change in C_{n_β} would be that observed. In the extreme case, the major vortex contribution would be on the same side of the twin vertical surfaces, initiating an asymmetric moment and resulting in an upset.

CONCLUDING REMARKS

The remotely piloted technique for obtaining flight test data on an unpowered 3/8-scale model of the F-15 airplane was found to provide adequate stability and control derivatives. The remotely piloted technique provided an opportunity to test the mathematical model in an angle of attack regime not previously examined in flight test. The derivatives were obtained for an angle of attack range from -20° to

53°. The variations of the estimates with angle of attack were consistent for most of the derivatives, particularly when the estimates were supplemented by uncertainty levels.

Some of the derivatives displayed evidence of nonlinearities. The magnitude of the longitudinal control effectiveness derivative for moderately high angles of attack was larger for small control surface deflection maneuvers than for large control surface deflection maneuvers. In addition, the directional stability derivative appeared to be double valued at an angle of attack near 38°. This may have resulted from asymmetric flow from the model's forebody.

Flight Research Center
National Aeronautics and Space Administration
Edwards, California 93523
October 3, 1975

REFERENCES

1. Holleman, Euclid C.: Summary of Flight Tests To Determine the Spin and Controllability Characteristics of a Remotely Piloted, Large-Scale (3/8) Fighter Airplane Model. NASA TN D-8052, 1976.

2. Edwards, John W.; and Deets, Dwain A.: Development of a Remote Digital Augmentation System and Application to a Remotely Piloted Research Vehicle. NASA TN D-7941, 1975.

3. Iliff, Kenneth W.; and Taylor, Lawrence W., Jr.: Determination of Stability Derivatives From Flight Data Using a Newton-Raphson Minimization Technique. NASA TN D-6579, 1972.

4. Iliff, Kenneth W.; and Maine, Richard E.: Practical Aspects of Using a Maximum Likelihood Estimator. Methods for Aircraft State and Parameter Identification, AGARD-CP-172, May 1975, pp. 16-1 — 16-15.

5. Maine, Richard E.; and Iliff, Kenneth W.: A FORTRAN Program for Determining Aircraft Stability and Control Derivatives From Flight Data. NASA TN D-7831, 1975.

6. Nguyen, Luat T.: Evaluation of Importance of Lateral Acceleration Derivatives in Extraction of Lateral-Directional Derivatives at High Angles of Attack. NASA TN D-7739, 1974.

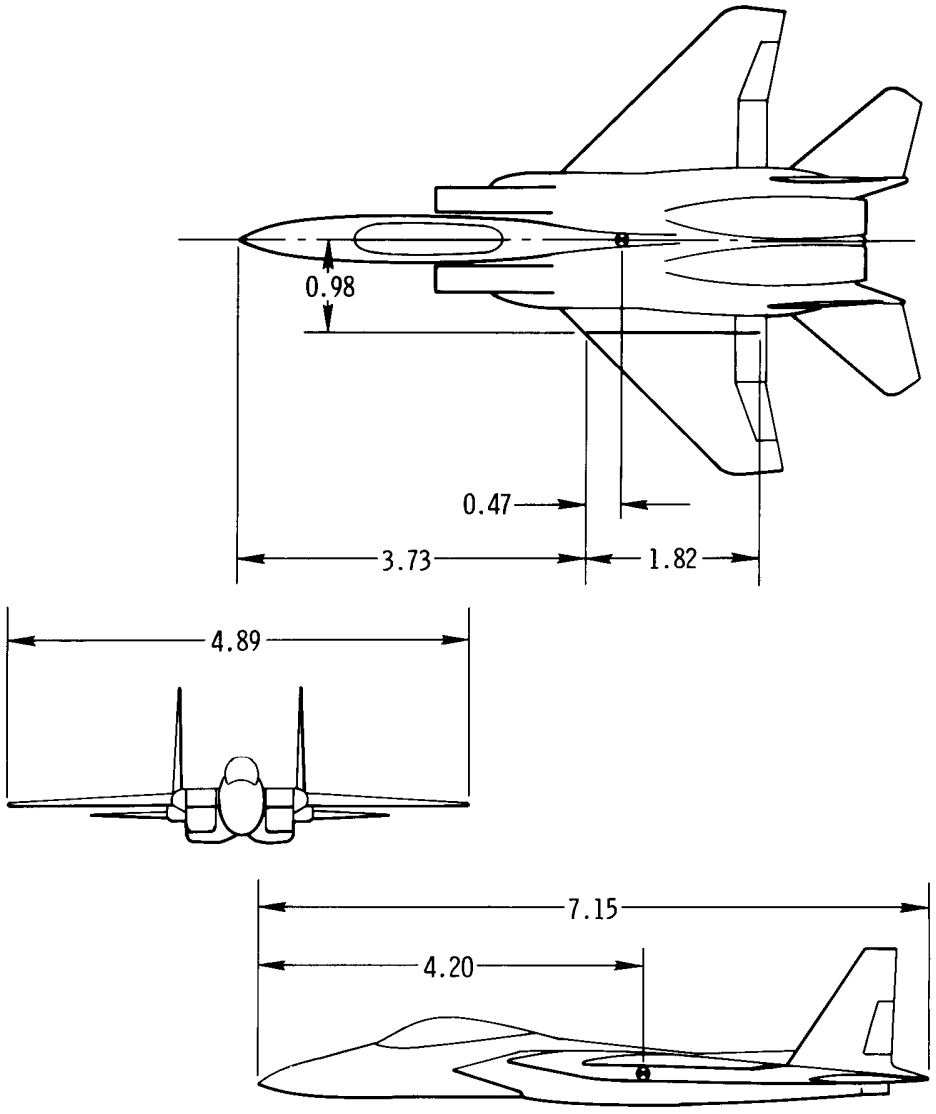

Figure 1. Three-view drawing of airplane model. Dimensions in meters.

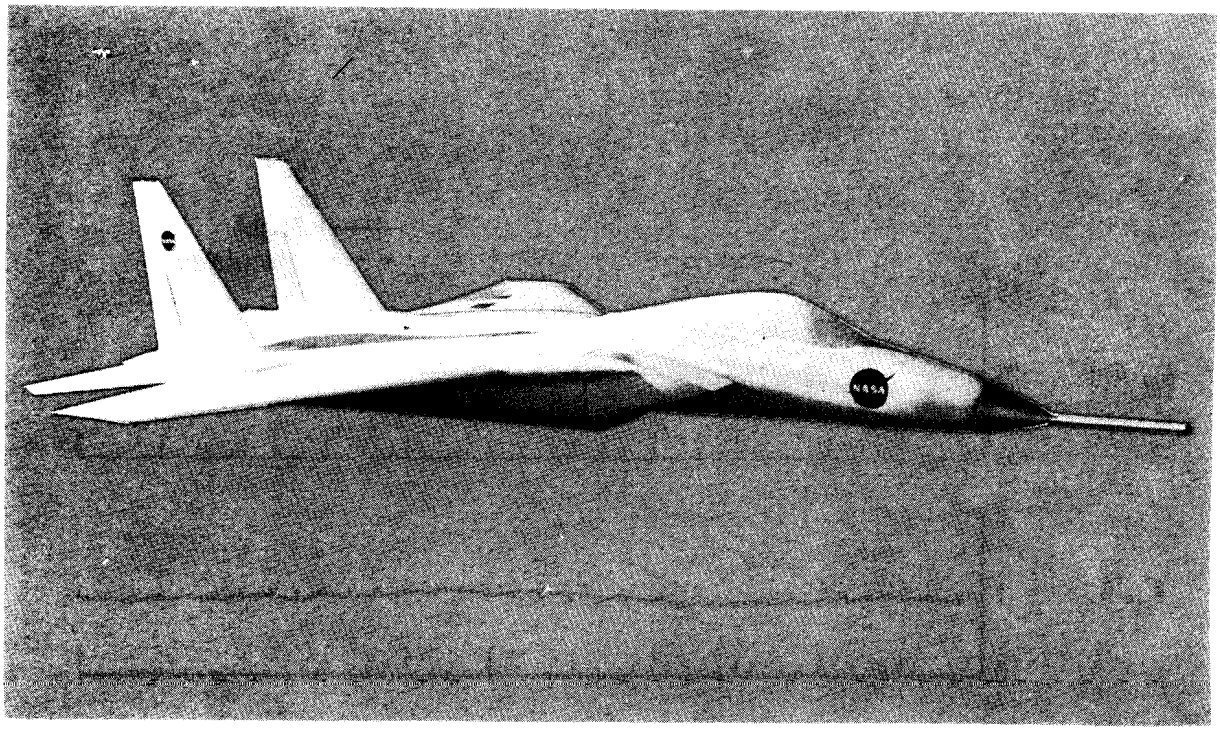

E-25487

Figure 2. Three-eighths-scale F-15 model.

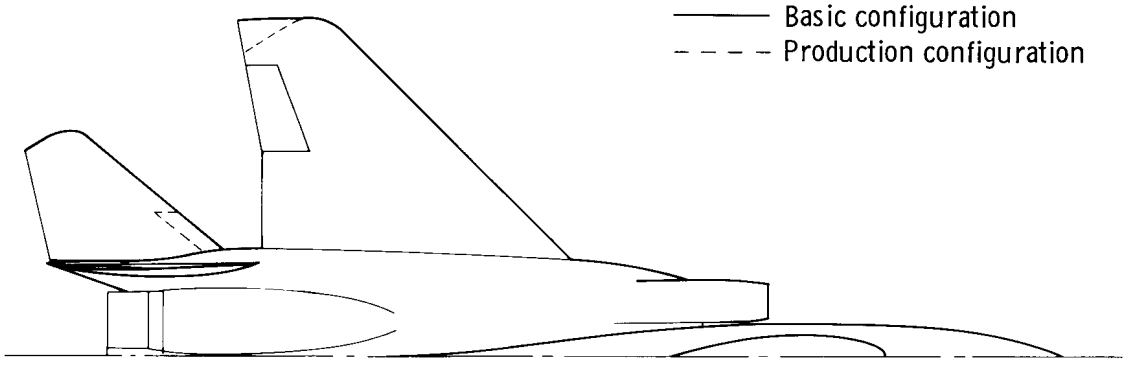

Figure 3. Basic and production configurations of the 3/8-scale model of the F-15 airplane.

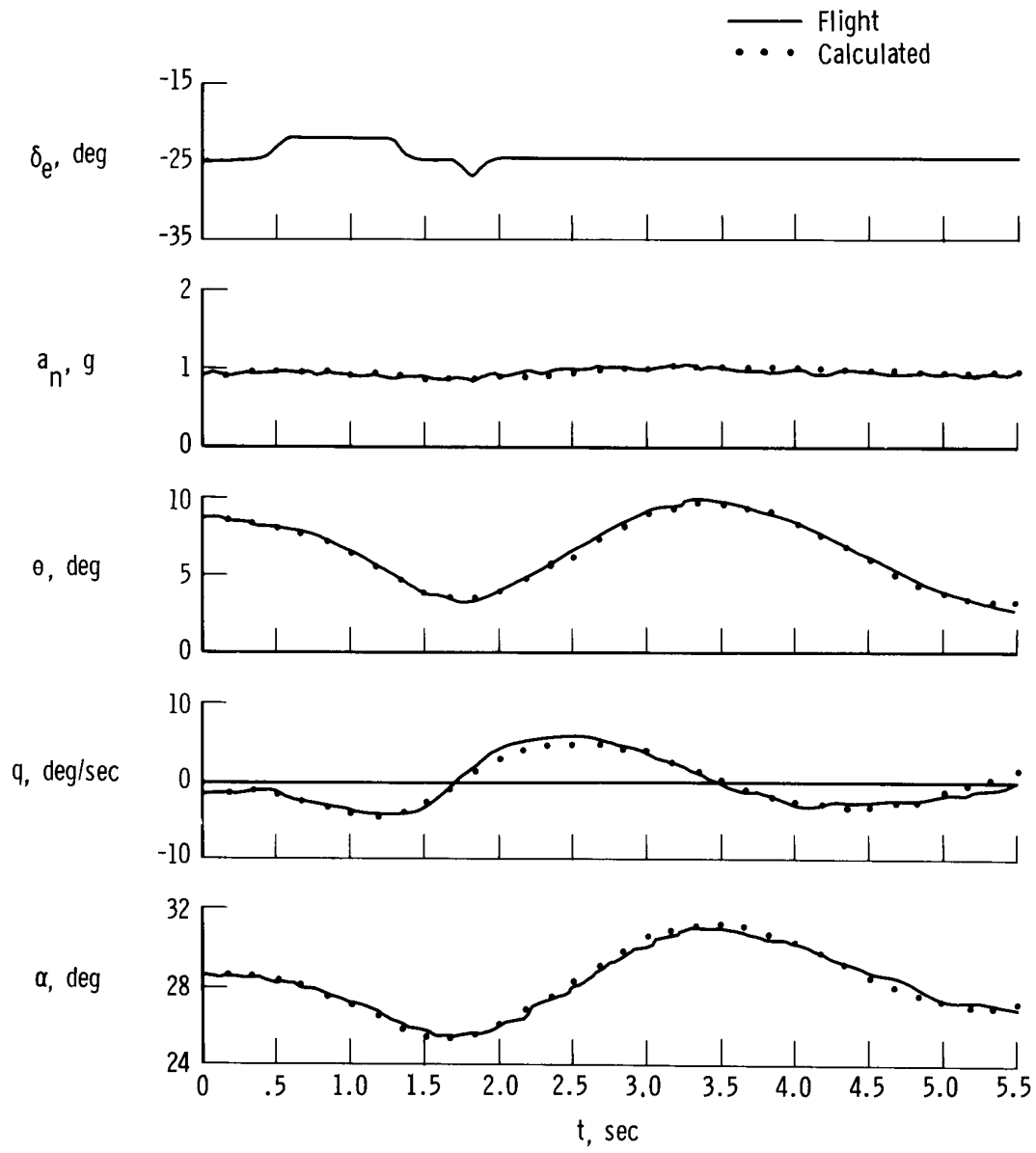

(a) Longitudinal maneuver.

Figure 4. Comparison of flight data and computed time histories based on the estimated derivatives for typical longitudinal and lateral-directional maneuvers.

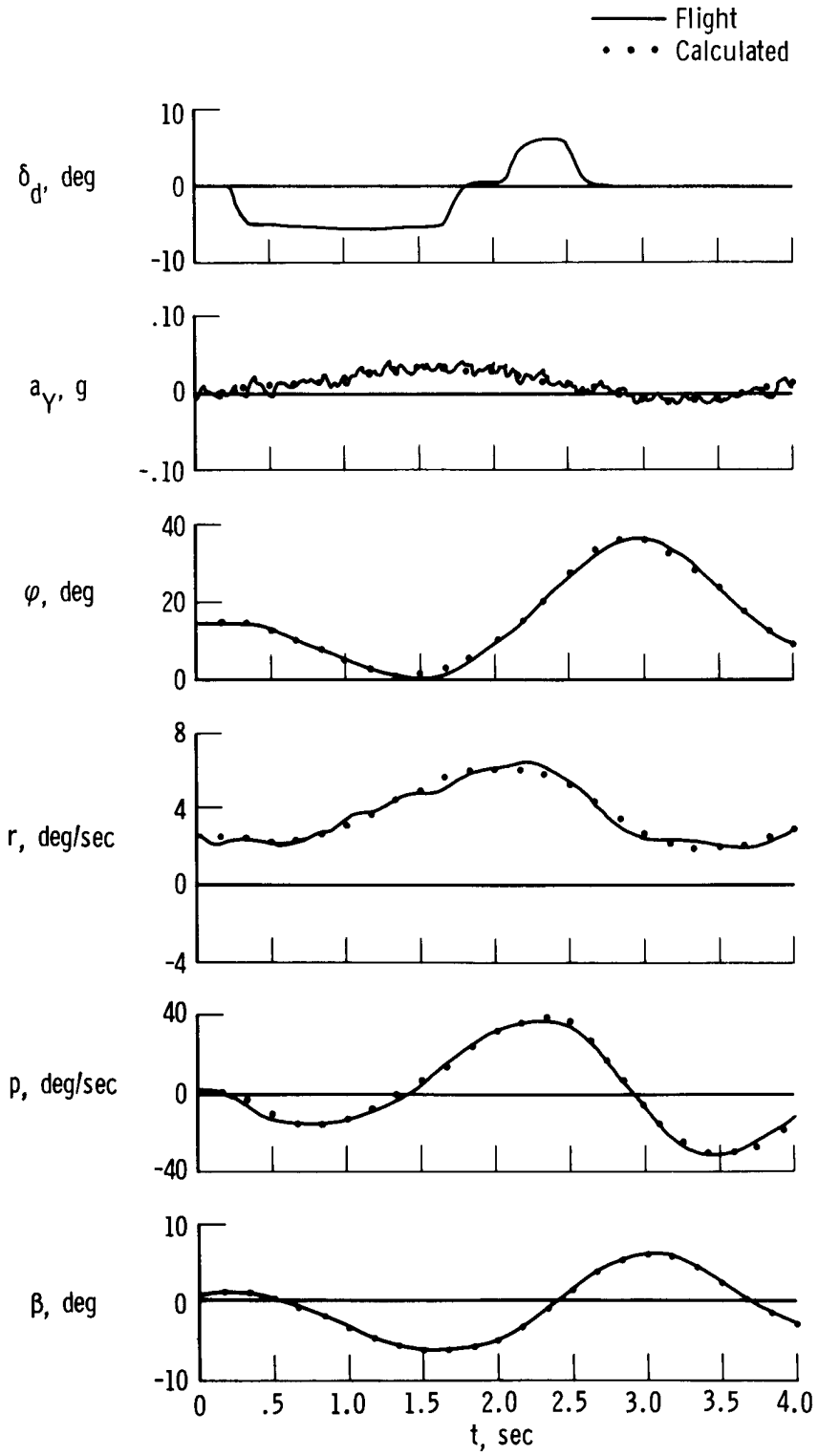

(b) Lateral maneuver, $\alpha = 23°$.

Figure 4. Concluded.

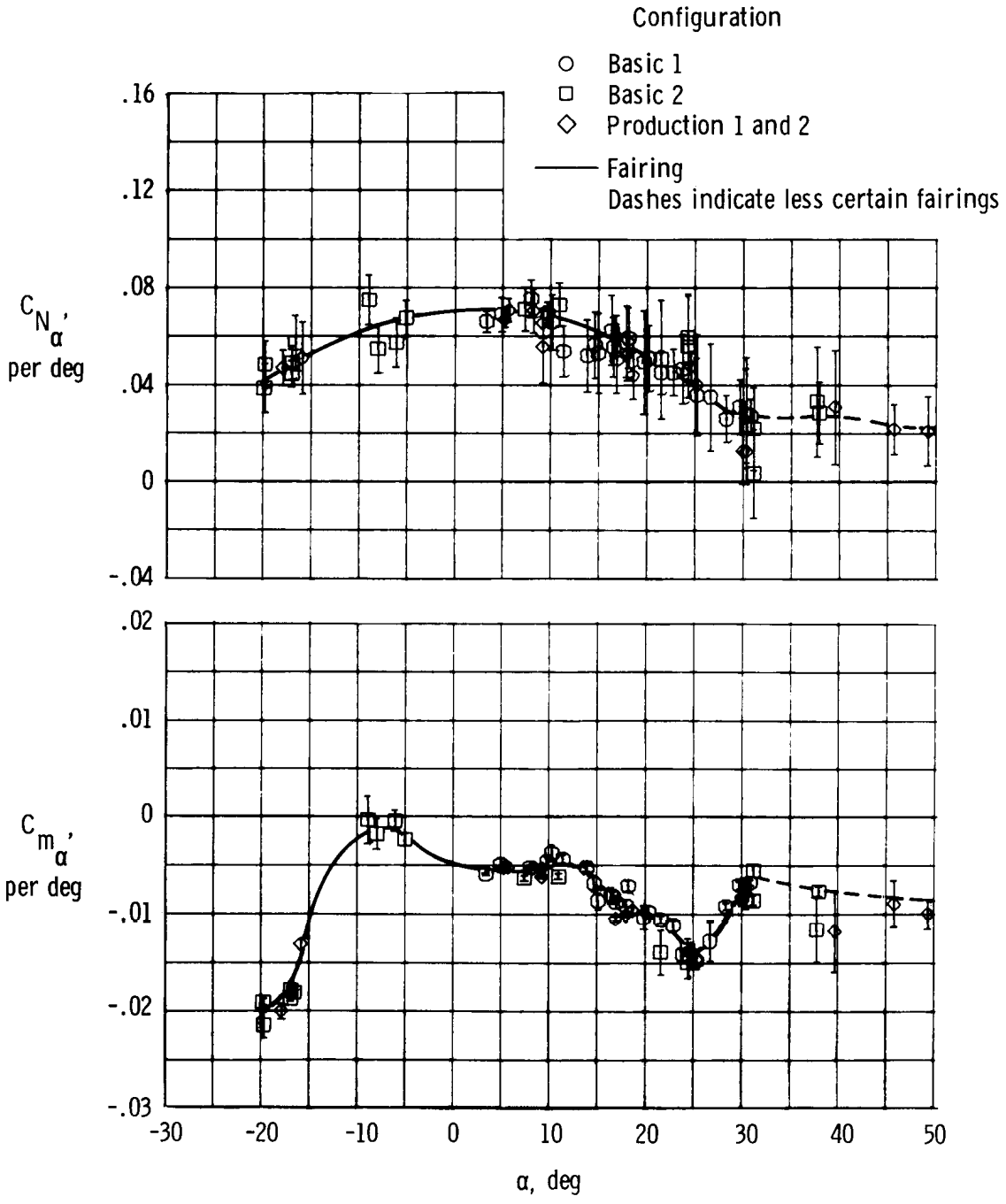

(a) C_{N_α}, C_{m_α}.

Figure 5. Subsonic longitudinal stability and control derivatives corrected to 26-percent mean aerodynamic chord.

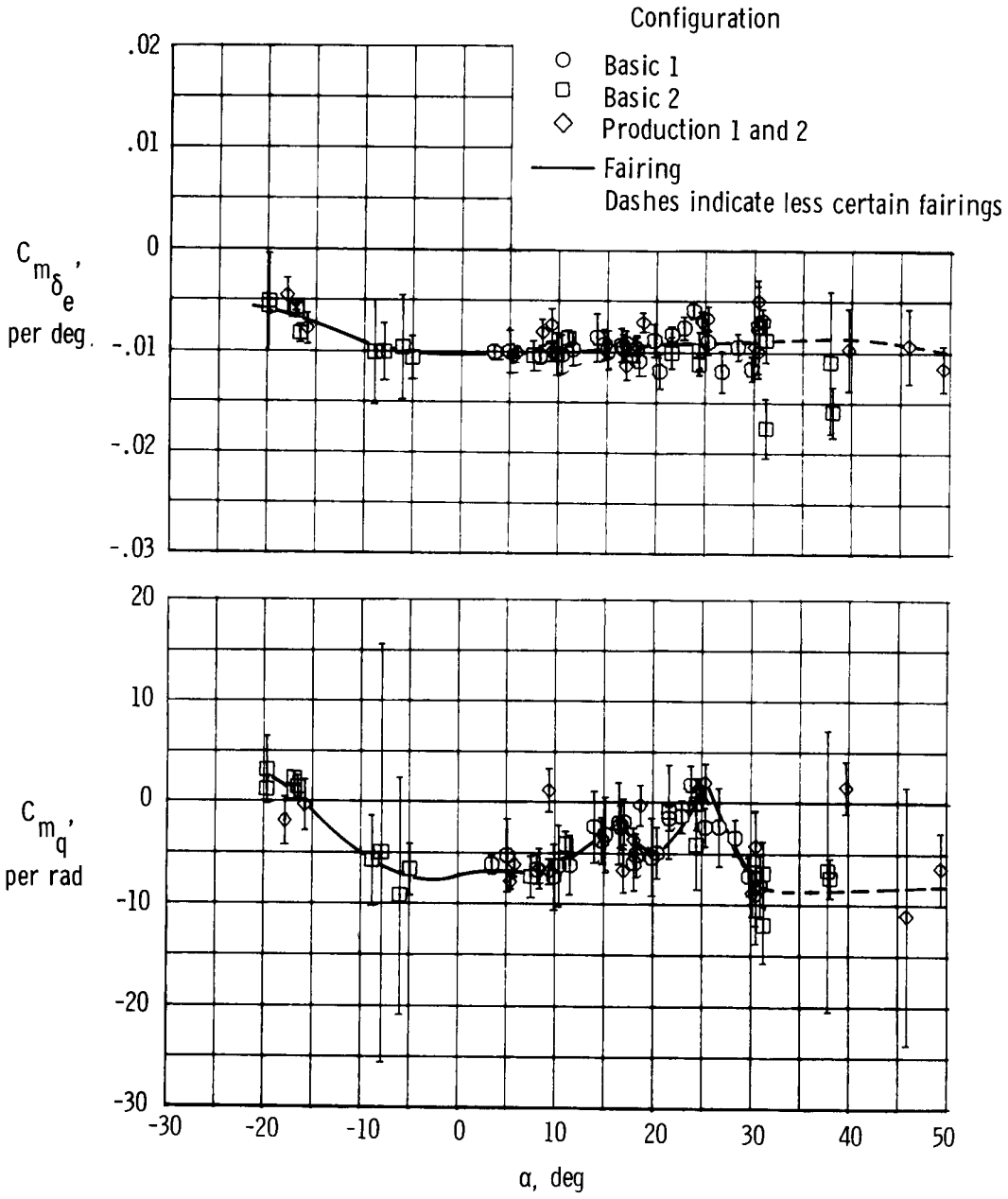

(b) $C_{m_{\delta_e}}$, C_{m_q}.

Figure 5. Continued.

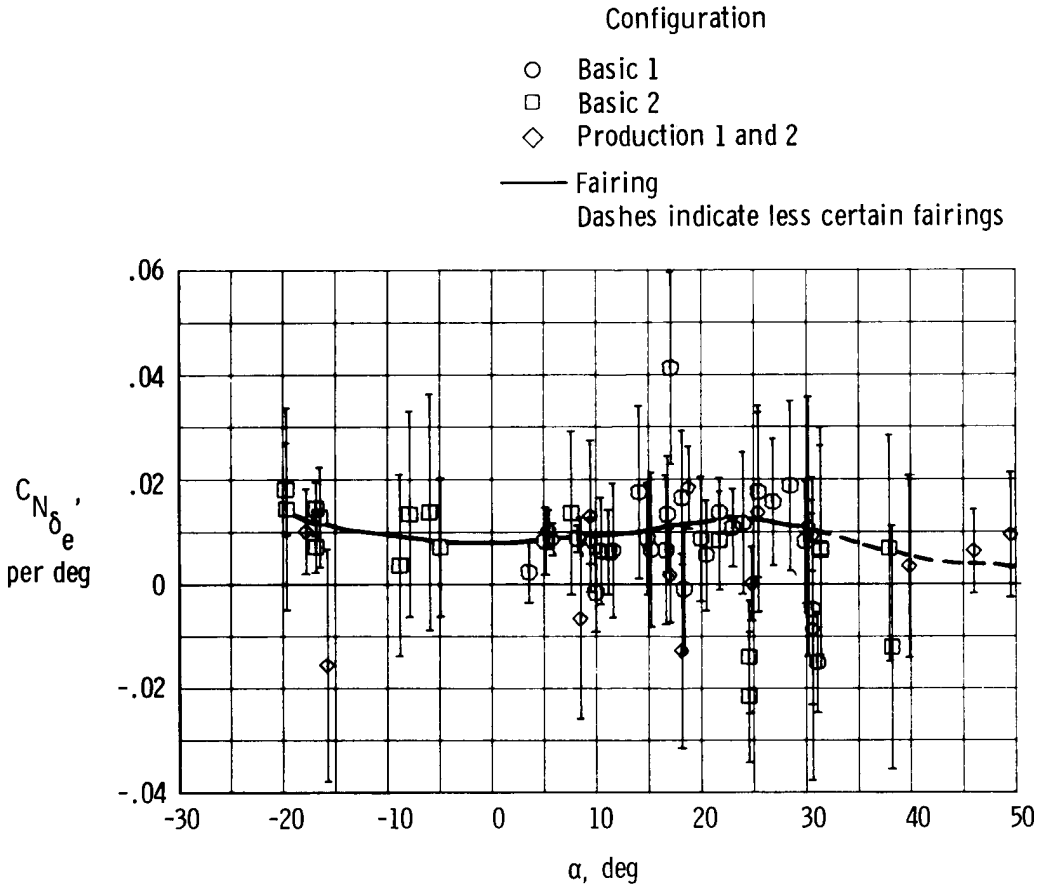

(c) $C_{N_{\delta_e}}$.

Figure 5. Continued.

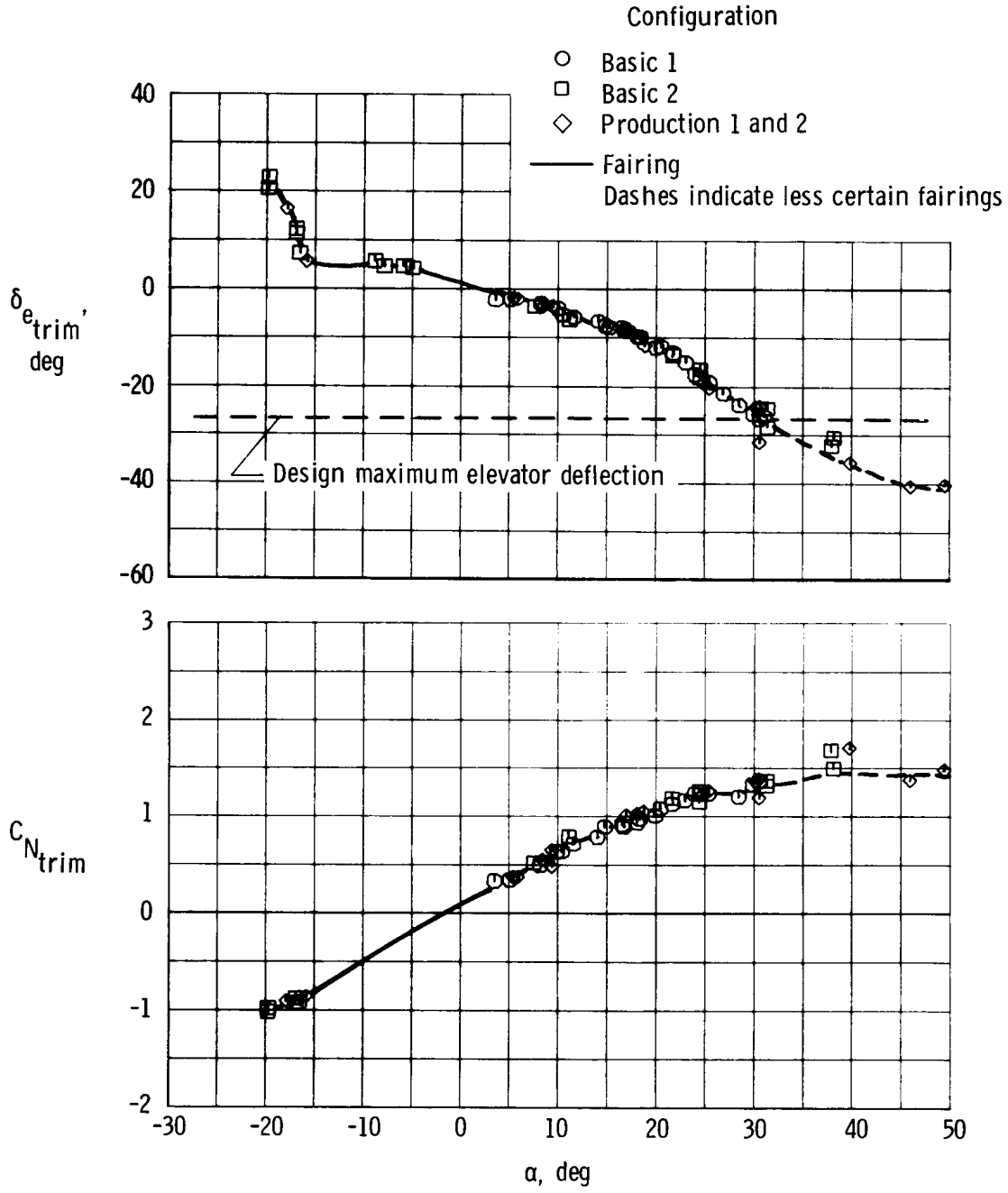

(d) $\delta_{e_{trim}}$, $C_{N_{trim}}$.

Figure 5. Concluded.

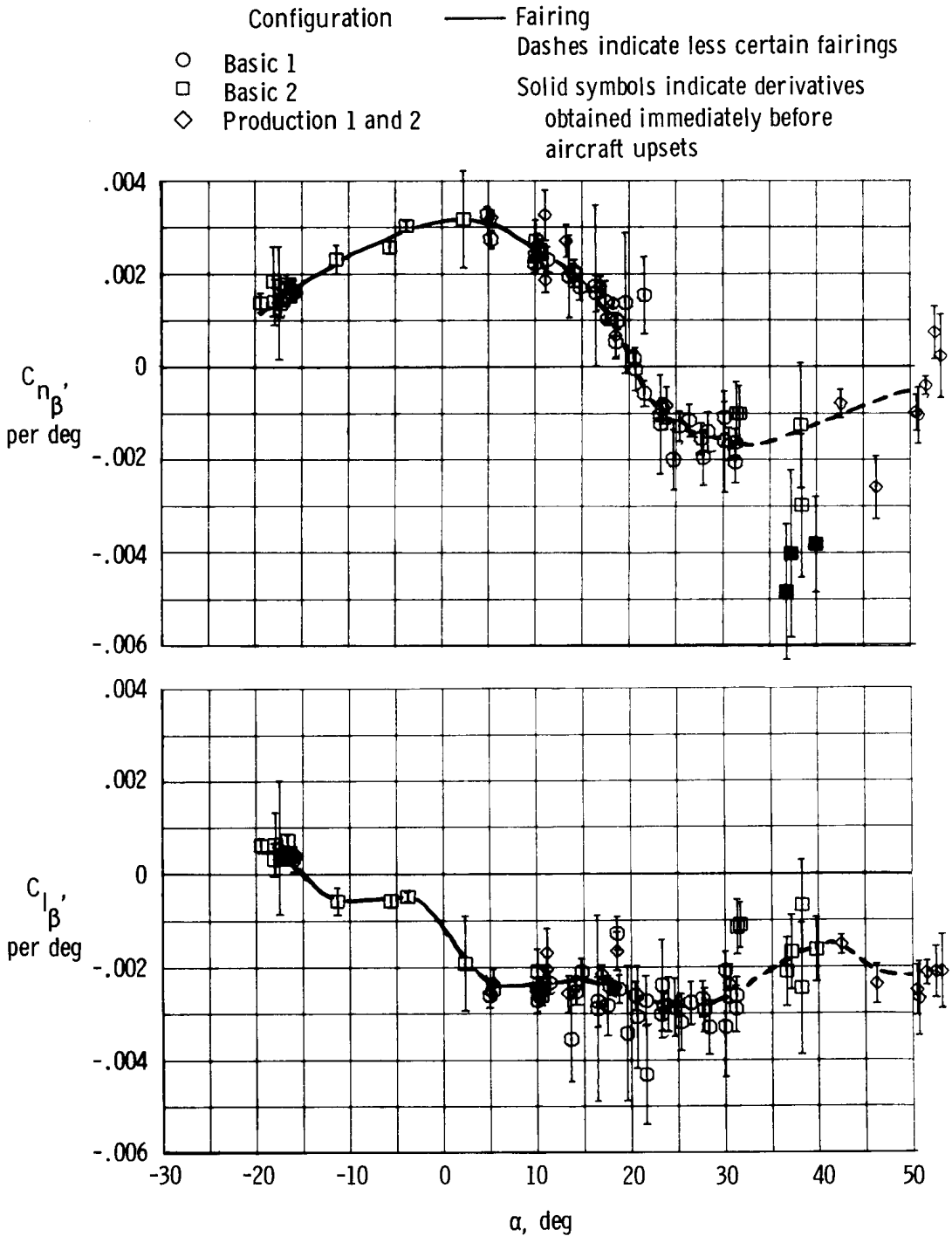

(a) C_{n_β}, C_{l_β}.

Figure 6. Subsonic lateral-directional stability and control derivatives corrected to 26-percent mean aerodynamic chord.

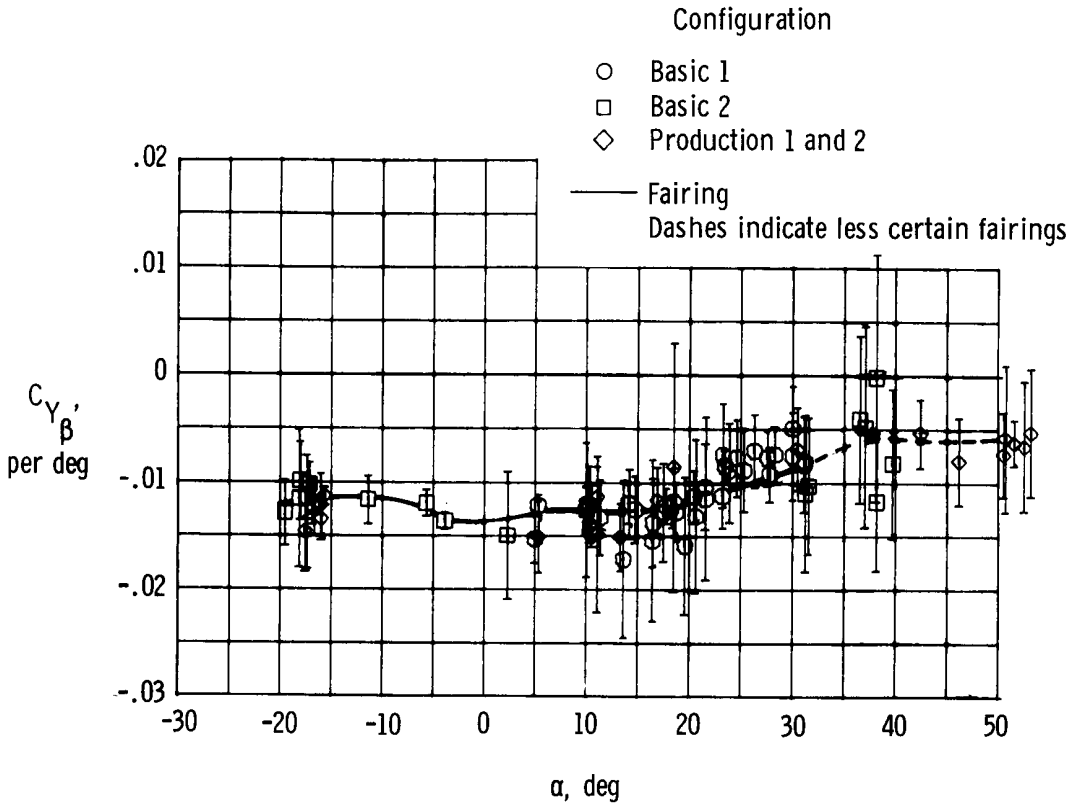

(b) C_{Y_β}.

Figure 6. Continued.

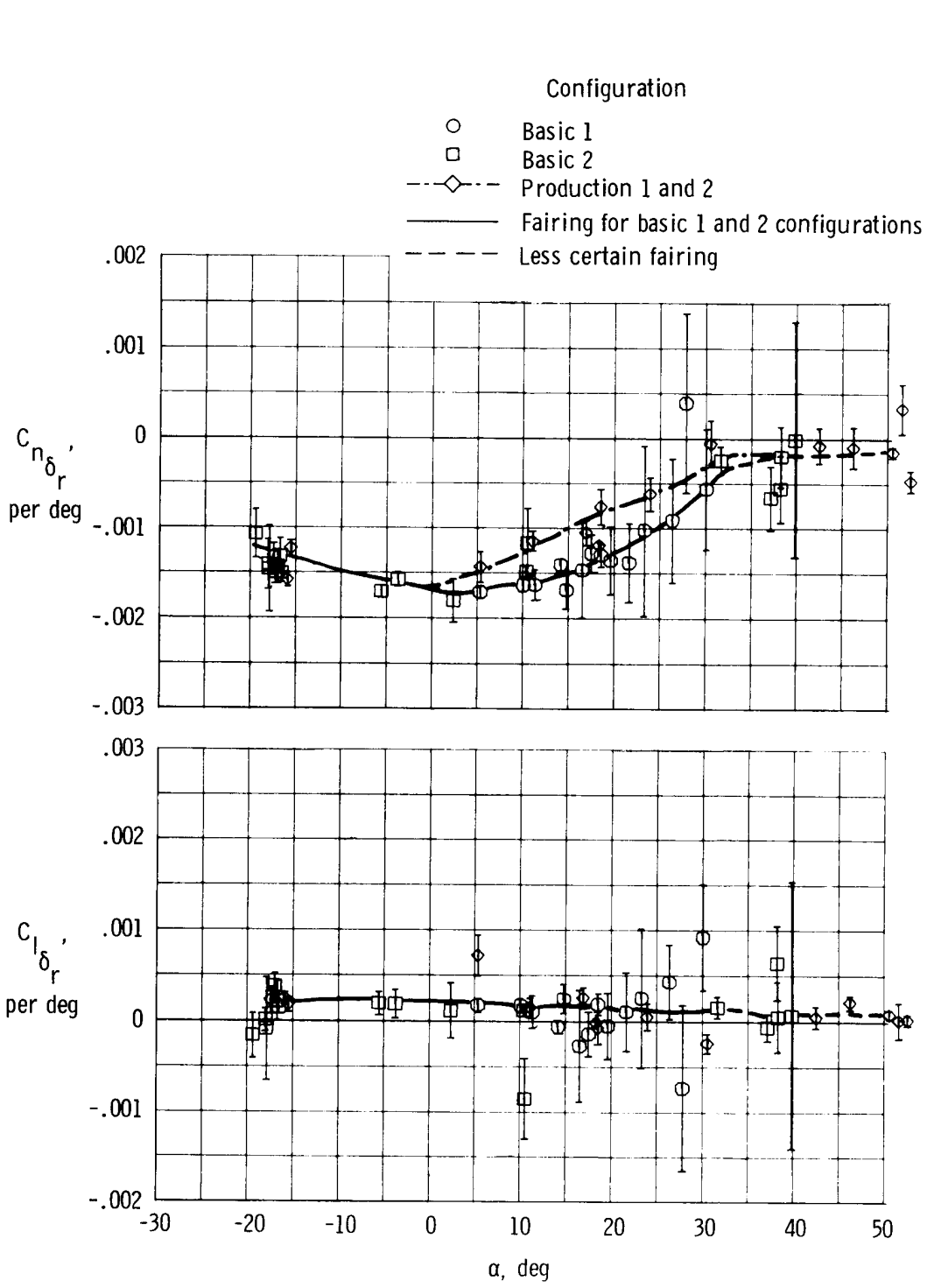

(c) $C_{n_{\delta_r}}$, $C_{l_{\delta_r}}$

Figure 6. Continued.

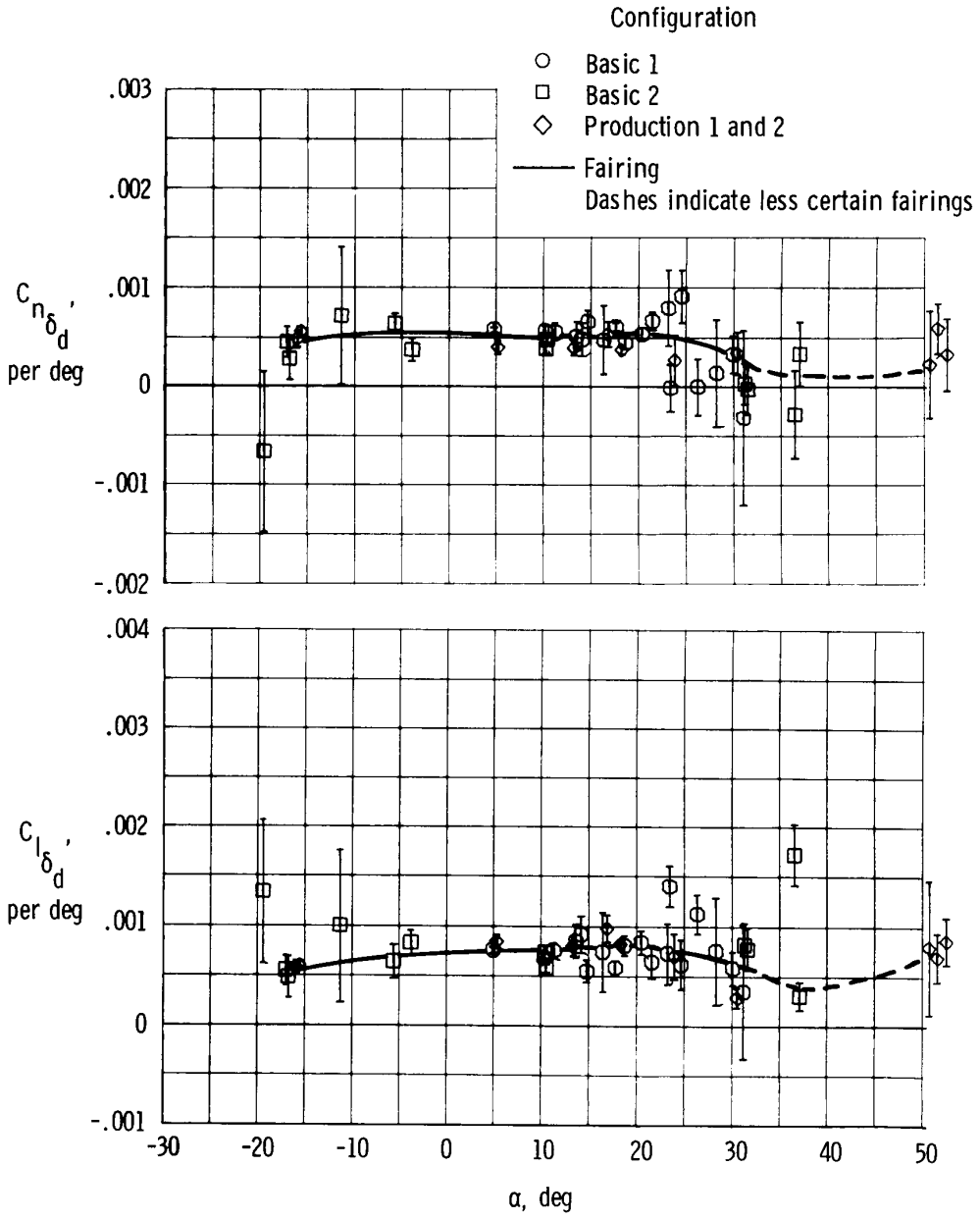

(d) $C_{n_{\delta_d}}$, $C_{l_{\delta_d}}$.

Figure 6. Continued.

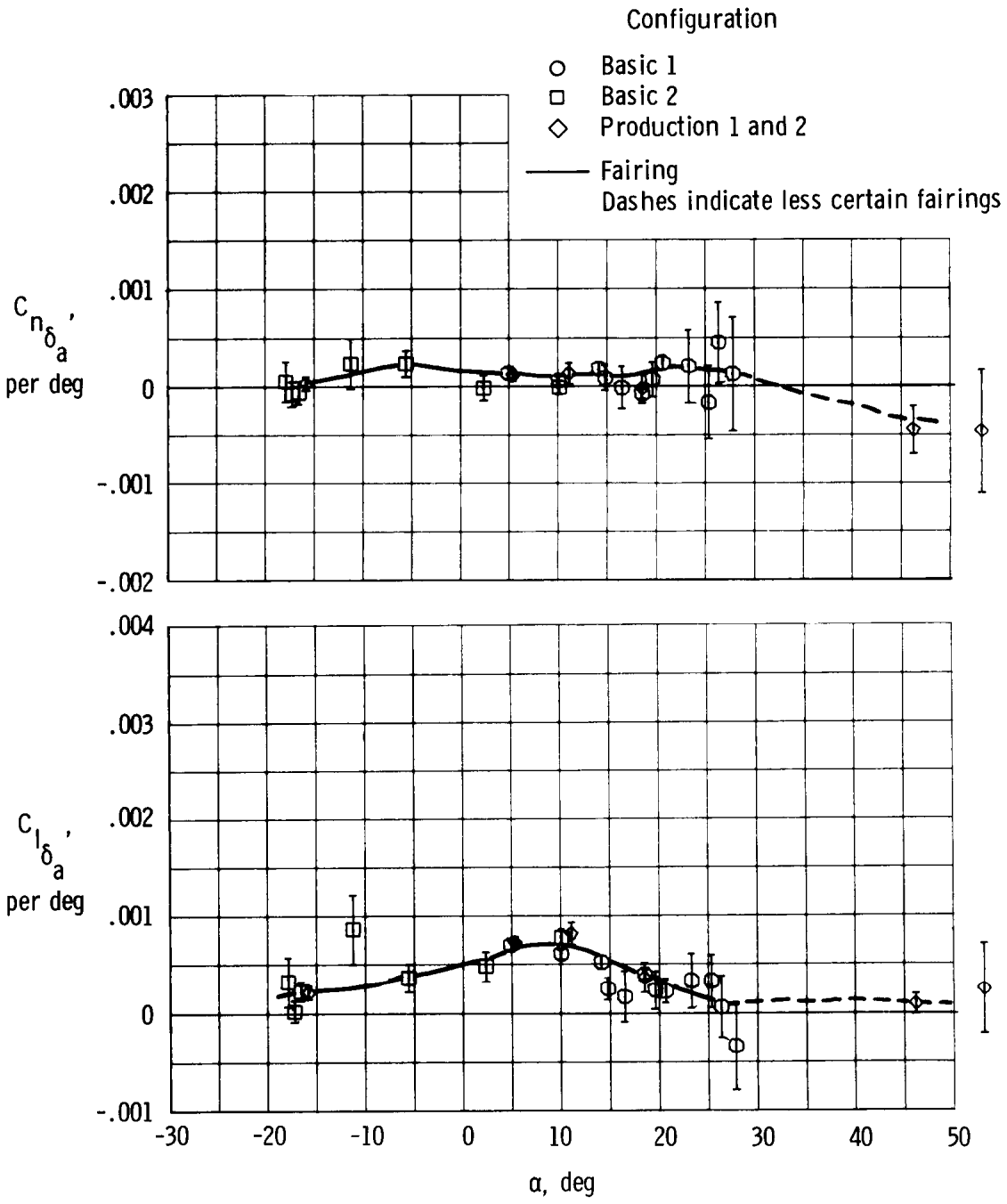

(e) $C_{n_{\delta_a}}$, $C_{l_{\delta_a}}$.

Figure 6. Continued.

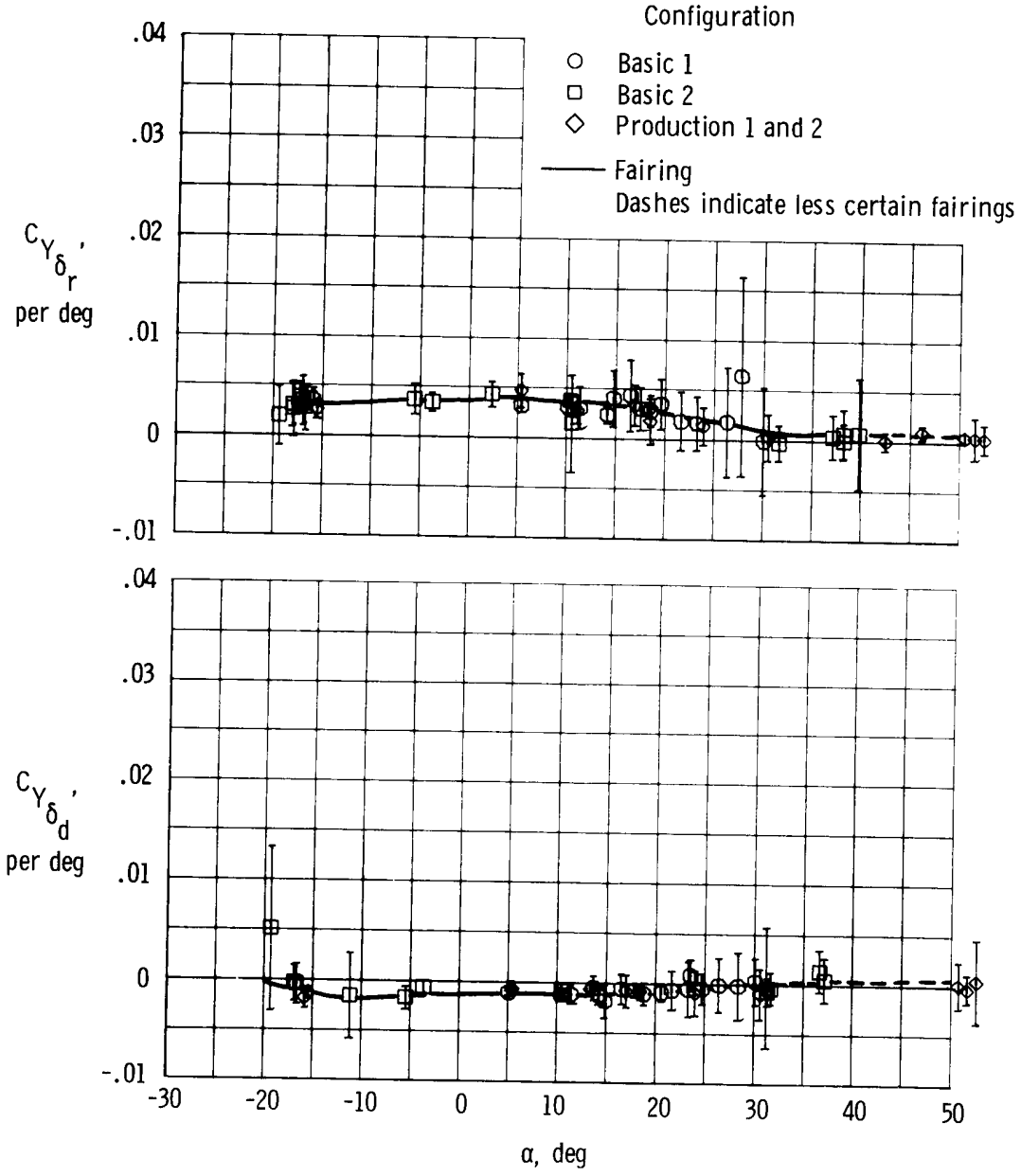

(f) $C_{Y_{\delta_r}}$, $C_{Y_{\delta_d}}$.

Figure 6. Continued.

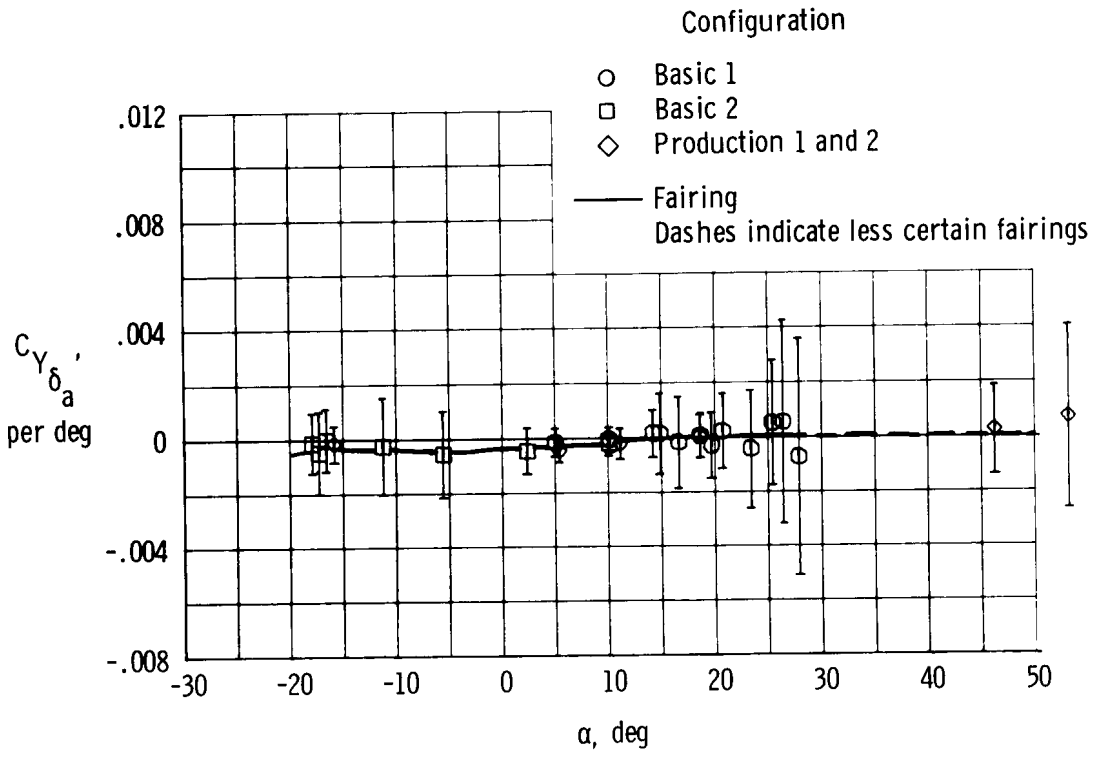

(g) $C_{Y_{\delta_a}}$.

Figure 6. Continued.

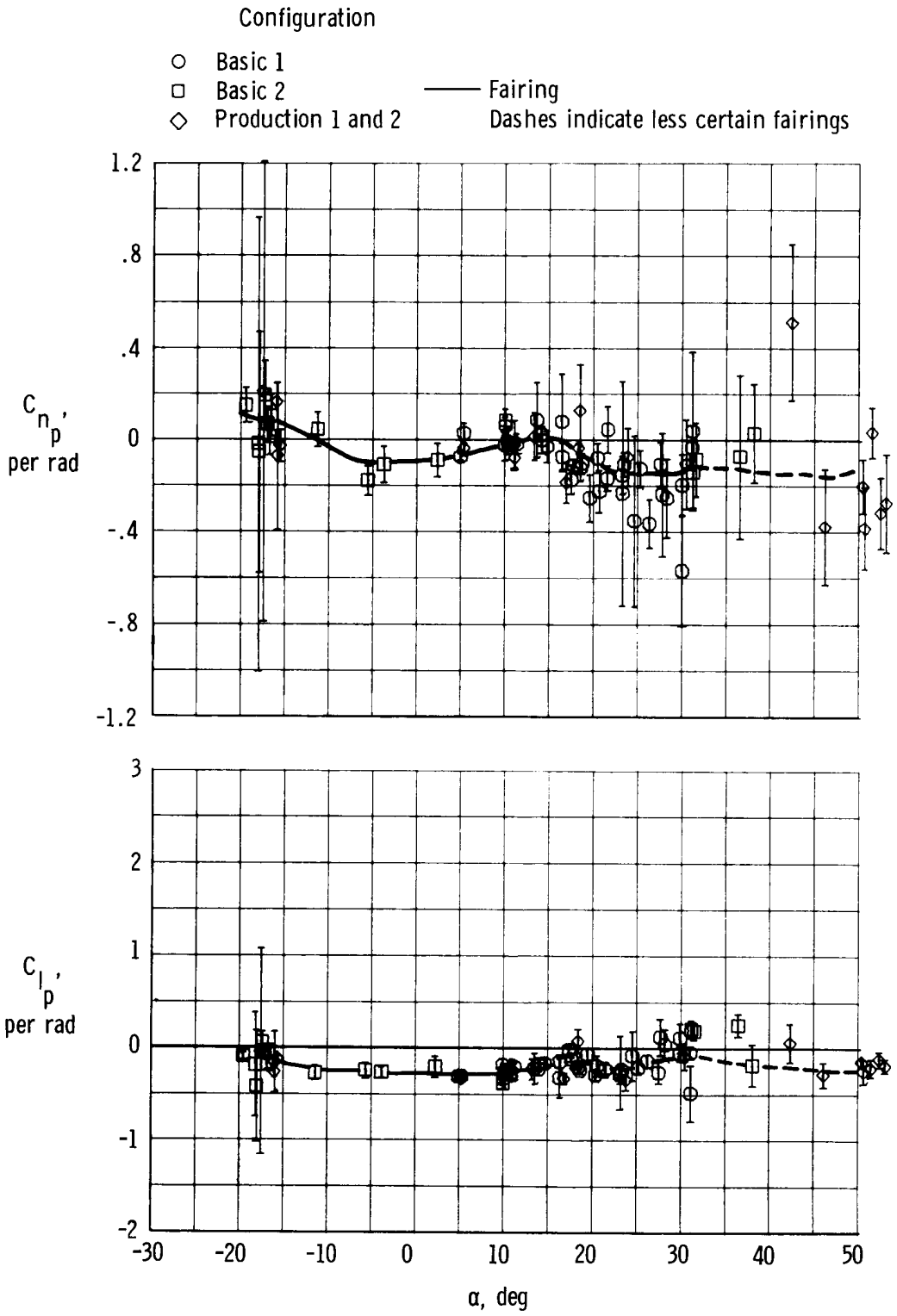

(h) C_{n_p}, C_{l_p}.

Figure 6. Continued.

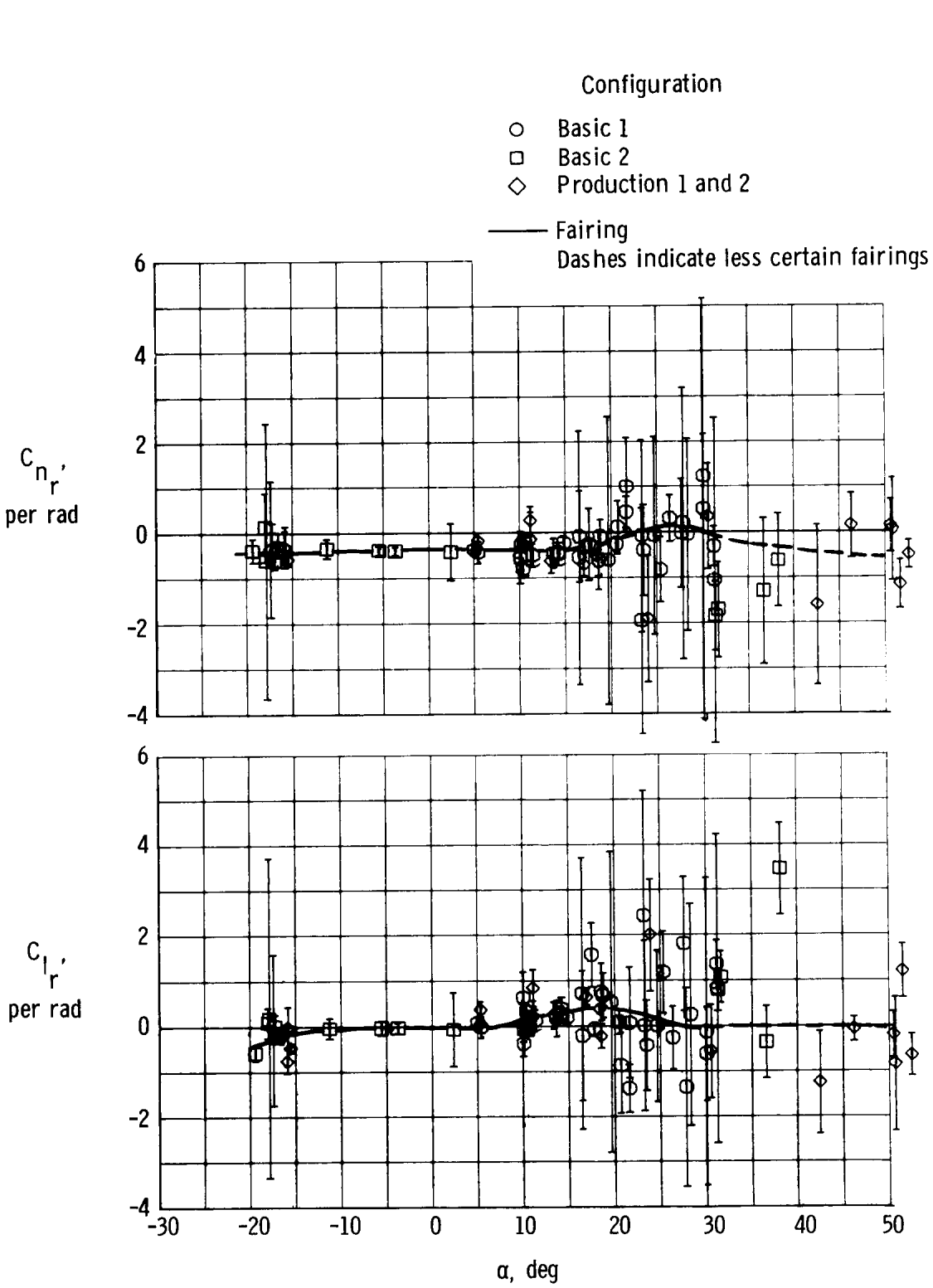

(i) C_{n_r}, C_{l_r}.

Figure 6. Continued.

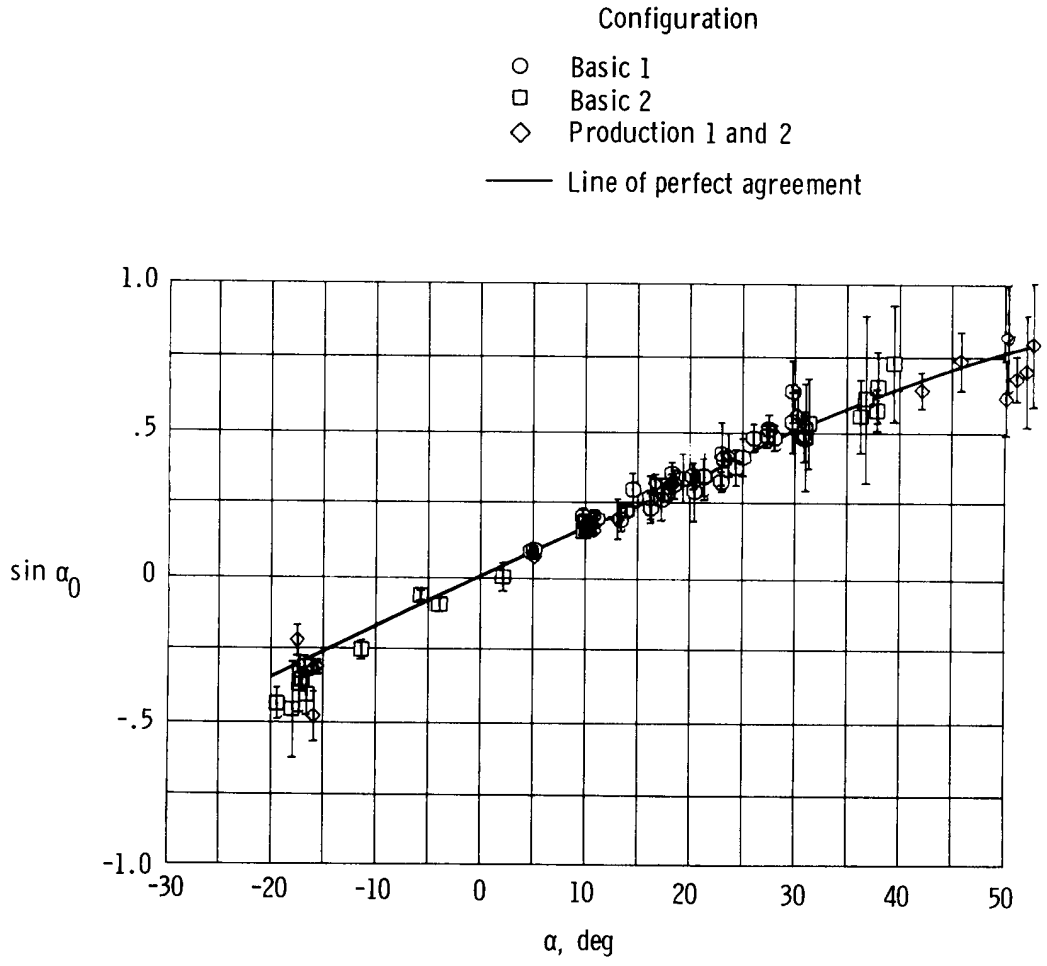

(j) Sin α_0.

Figure 6. Concluded.